AGU PUBLICATIONS

JGR

Journal of Geophysical Research: Oceans

RESEARCH ARTICLE

10.1002/2016JC012158

Key Points:
- Denmark Strait Overflow Water has three main sources
- Water mass transformation north of Iceland feeds the North Icelandic Jet
- Wind stress anomalies around Iceland cause volume and freshwater transport variations

Supporting Information:
- Supporting Information S1

Correspondence to:
E. Behrens,
erik.behrens@niwa.co.nz

Citation:
Behrens, E., K. Våge, B. Harden, A. Biastoch, and C. W. Böning (2017), Composition and variability of the Denmark Strait Overflow Water in a high-resolution numerical model hindcast simulation, *J. Geophys. Res. Oceans*, *122*, doi:10.1002/2016JC012158.

Received 18 JUL 2016
Accepted 6 MAR 2017
Accepted article online 11 MAR 2017

Composition and variability of the Denmark Strait Overflow Water in a high-resolution numerical model hindcast simulation

Erik Behrens[1], Kjetil Våge[2], Benjamin Harden[3], Arne Biastoch[4], and Claus W. Böning[4]

[1]National Institute for Water and Atmospheric Research, Wellington, New Zealand, [2]Geophysical Institute, Bjerknes Centre for Climate Research, University of Bergen, Bergen, Norway, [3]Woods Hole Oceanographic Institution, Woods Hole, Massachusetts, USA, [4]GEOMAR—Helmholtz Centre for Ocean Research Kiel, Kiel, Germany

Abstract The upstream sources and pathways of the Denmark Strait Overflow Water and their variability have been investigated using a high-resolution model hindcast. This global simulation covers the period from 1948 to 2009 and uses a fine model mesh (1/20°) to resolve mesoscale features and the complex current structure north of Iceland explicitly. The three sources of the Denmark Strait Overflow, the shelfbreak East Greenland Current (EGC), the separated EGC, and the North Icelandic Jet, have been analyzed using Eulerian and Lagrangian diagnostics. The shelfbreak EGC contributes the largest fraction in terms of volume and freshwater transport to the Denmark Strait Overflow and is the main driver of the overflow variability. The North Icelandic Jet contributes the densest water to the Denmark Strait Overflow and shows only small temporal transport variations. During summer, the net volume and freshwater transports to the south are reduced. On interannual time scales, these transports are highly correlated with the large-scale wind stress curl around Iceland and, to some extent, influenced by the North Atlantic Oscillation, with enhanced southward transports during positive phases. The Lagrangian trajectories support the existence of a hypothesized overturning loop along the shelfbreak north of Iceland, where water carried by the North Icelandic Irminger Current is transformed and feeds the North Icelandic Jet. Monitoring these two currents and the region north of the Iceland shelfbreak could provide the potential to track long-term changes in the Denmark Strait Overflow and thus also the AMOC.

1. Introduction

The Nordic Seas are a key region for Europe's climate where warm and salty waters of subtropical origin, carried by the Atlantic Meridional Overturning Circulation (AMOC), meet cold and fresh water from the Arctic Ocean [*Orvik and Niiler*, 2002; *Glessmer et al*., 2014]. The densest portion of the North Atlantic Deep Water (NADW), a source to the lower limb of the AMOC, is formed in this region [*Dickson and Brown*, 1994]. This dense water outflow is constrained by Greenland-Scotland Ridge offering three deep passages to the south: the Denmark Strait, the Faroe Bank Channel, and the Iceland-Faroe Ridge. The Denmark Strait Overflow Water (DSOW) is the largest of the overflow plumes from the Nordic Seas [*Jochumsen et al*., 2012] and provides the densest contribution to the Deep Western Boundary Current (DWBC) which can be tracked all along the east coast of the American continent [*Send et al*., 2011; *Mertens et al*., 2014; *Fischer et al*., 2015].

Long-term transport measurements have been carried out in the Denmark Strait over the past decades [*Macrander et al*., 2007; *Jochumsen et al*., 2012, 2015], but details of where and how the DSOW is formed are still incomplete. In the past, open ocean convection in the Iceland and Greenland Seas has been thought to be the dominant source for the DSOW [*Swift et al*., 1980; *Swift and Aagaard*, 1981] before the transformation of warm and salty water within the eastern part of the Nordic Seas was identified as the primary source [*Mauritzen*, 1996]. Lately another significant source of the DSOW has been discovered north of Iceland [*Jónsson*, 2004], which is now known as the North Icelandic Jet (NIJ) [*Våge et al*., 2011]. Further light on the DSOW and its sources and variability were shed by repeated hydrographic surveys and a mooring array deployed north of the Denmark Strait across the Kögur section [*Våge et al*., 2013; *de Steur et al*., 2016; *Harden et al*., 2016]. They reported mean overflow ($\sigma_0 > 27.8$ kg/m^3) transports for the shelfbreak EGC, the separated EGC, and the NIJ of about 1.5, 1, and 1 Sv, respectively, and a mean liquid freshwater transport across

this section of 65 mSv. At the northern end of the Blosseville Basin, the EGC bifurcates into two branches; the shelfbreak branch follows the Greenland shelfbreak and the separated branch flows along the deep slope of Iceland toward Denmark Strait. Based on hydrographic surveys along the Iceland slope and idealized numerical model simulations, the existence of a local overturning loop which involves boundary current system north of Iceland, the NIJ and the North Icelandic Irminger Current (NIIC), and water mass transformation in the Iceland Sea was hypothesized [*Våge et al*., 2011].

Earlier modeling studies suggested a complex circulation north of the Denmark Strait [*Köhl et al*., 2007; *Köhl*, 2010; *Logemann et al*., 2013]. It has been established that local wind forcing is the main driver for variability in volume transport across the Kögur section and across the Denmark Strait [*Biastoch et al*., 2003; *Köhl et al*., 2007; *Köhl*, 2010; *Logemann et al*., 2013; *Yang and Pratt*, 2014; *Harden et al*., 2016]. Increased wind stress curl (positive North Atlantic Oscillation) enhances the flow along the Greenland slope, while weaker wind stress curl (negative North Atlantic Oscillation) strengthens the flow along the Iceland slope [*Köhl*, 2010]. However, links between the NAO conditions and transport variability are not fully understood. Positive NAO phases have been related to enhanced overflow transport across Denmark Strait while, for negative NAO conditions, no clear link has been found [*Jochumsen et al*., 2012]. Furthermore, recent measurements linked changes in the shelfbreak and separated EGC branches to wind-driven changes in the Blosseville Basin [*Våge et al*., 2013; *Harden et al*., 2016]. Here a stronger shelfbreak branch weakens the contribution of the separated EGC to the overflow plume and vice versa.

Previous high-resolution regional modeling studies [*Köhl et al*., 2007; *Logemann et al*., 2013; *Yang and Pratt*, 2014] were constrained by boundary conditions, data assimilation and usually short simulation periods of up to 10 years. Their horizontal resolution of about $\sim$7 km in the Denmark Strait region permitted partial resolution of mesoscale eddies [*Köhl et al*., 2007; *Logemann et al*., 2013]. Even finer grid sizes ($<$1/16° around Iceland) are required to capture them fully [*Chelton et al*., 2007; *Hallberg*, 2013]. It has been found that these mesoscale eddies cause the largest transport variability in the overflow through Denmark Strait [*Jochumsen et al*., 2012], highlighting two of the remaining open questions in the region: what triggers variability in the overflow and on what time scale? So far models and observation have not come to a consensus. Models show a distinctly larger seasonal variability compared to observations [*Köhl et al*., 2007; *Jochumsen et al*., 2012] and the link to the NAO on interannual time scales is not fully understood. This leaves questions on the driving mechanism quite open.

The aim of this study is to re-evaluate and extend earlier model findings using a more sophisticated 60 year long global model hindcast with grid sizes of only about 3 km in this region in combination with Lagrangian trajectory analyses to investigate the sources of the DSOW and their variability from seasonal to interannual time scale. Results of this model hindcast [*Behrens*, 2013; *Böning et al*., 2016] also help to place the recently observed transport time series across the Kögur section over a short period [*de Steur et al*., 2016; *Harden et al*., 2016] into a larger perspective in terms of seasonal to interannual variability. In addition, we aim to shed new light on the local overturning loop north of Iceland [*Våge et al*., 2011]. This has not previously been done in a realistic model setup.

The manuscript is structured as follows: section 2 contains the description of the model and model hindcast. In addition to this, relevant diagnostics will be introduced. Section 3 provides the main results and findings of this investigation before a conclusion is provided in section 4.

2. Methods

In this study, we use output of a novel high-resolution (1/20°) model hindcast over the period 1948–2009, which is based on the ocean model NEMO [*Madec*, 2008] and sea ice model LIM2-VP [*Fichefet and Maqueda*, 1997] within the international DRAKKAR-framework (http://www.drakkar-ocean.eu/). This model configuration (VIKING20) utilizes a global 0.25° domain (ORCA025, tri-polar grid) and local grid refinement (AGRIF) [*Debreu et al*., 2008] of 1/20° covering the North Atlantic and Nordic Seas, between 32°N and 85°N. Details of this configuration can be found in *Behrens* [2013] and *Böning et al*. [2016]. The vertical grid uses 46 z-levels, with increasing layer thicknesses with depth from 6 m at the surface to 250 m below 1000 m. A partial cell approach is used to improve the representation of flows over sloping bottom topography [*Barnier et al*., 2006].

This model hindcast is forced with interannually varying forcing fields based on CORE.v2 [*Large and Yeager*, 2009], which covers the period 1948–2009. The precipitation north of ~62° has been artificially reduced, by 10%, to take uncertainties in the surface freshwater fluxes of CORE.v2 into account and reduce the long-term drift in water masses [*Behrens et al*., 2013]. The coastal freshwater flux (river runoff) uses estimates of *Dai and Trenberth* [2002], with some slight modifications, as described in *Bourdallé-Badie and Treguier* [2006]. Sea surface salinity (SSS) has been very weakly restored with a piston velocity of 16.4 mm/d and an additional limitation of $\Delta SSS = 0.5$ toward climatology. No restoring has been applied within a swath (~100 km width) around the Greenland coast. The model output of this configuration has been stored in 5 day means over the entire simulation period. The diagnostic time series shown in this manuscript start in 1960 to avoid possible spin-up effects that may have taken place in the first 12 years.

A Lagrangian particle tracking tool (Ariane) [*Blanke et al*., 1999] has been utilized to investigate the sources of the DSOW and to investigate the local overturning loop (which feeds the NIJ). The 5 day mean model velocity fields have been used to calculate model trajectories offline. Particles were continuously seeded backward in time along the entire Denmark Strait section (red line in Figure 1a), with potential densities (σ_0) larger than 28.0 kg/m^3 (transport depending) over the period from 2000 to 2009 representing our reference period. We deliberately choose the 28.0 kg/m^3 surface as the classical 27.8 kg/m^3 surface shows large vertical movement and makes a clear interpretation of trajectories more challenging. Our Denmark Strait section follows the model grid accurately to consistently compute transports and to seed particles using the built-in function of the trajectory tool. This means that the Denmark Strait section is not a straight line and includes part of the Kangerlussuaq Trough. However, in this manuscript, we only include particles seeded east of 29.5°W, in the deepest part of the Denmark Strait and with velocities orientated away from the Nordic Seas. Every 2 days, the location (three-dimensional) and hydrographic properties of each particle were recorded to capture the particle trajectory in time. Every trajectory location has been used to compute a probability density by regridding them onto a regular $0.25° \times 0.25°$ latitude longitude grid, as done by *Gary et al*. [2011]. The same technique has also been applied to map the probabilities into Θ-S space, with $\Delta\Theta = 0.1°C$ and $\Delta S = 0.01$ intervals, based on the recorded temperature and salinity properties for each particle. In both diagnostics, the reoccupation of a position by the same particle has been excluded to highlight the particle pathways and not its "residence time."

Mean physical properties and transports have been evaluated across two sections (shown in Figure 1a). In addition to the Denmark Strait section, we use a slightly modified Kögur section (blue section in Figure 1) which is shifted northward compared to the hydrographic section described in *Våge et al*. [2013]. This northward shift enabled a clearer separation between the different overflow branches [*Harden et al*., 2016]. The model data are located on an Arakawa-C grid and have been subsampled along this section. Freshwater transports have been calculated using $S_{ref} = 34.8$ as a reference, guided by the recent work of *de Steur et al*. [2016].

3. Results

3.1. Velocity Field Upstream of the Denmark Strait

The mean velocity field upstream of the Denmark Strait for water on the 28.0 kg/m^3 sigma surface over the 2000–2009 period is shown in Figure 1. High flow speeds (>10 cm/s) are seen within the EGC along the Greenland shelfbreak, along the Iceland shelfbreak north of the Denmark Strait and in the Kangerlussuaq Trough (Figures 1a and 1b). East of the Scoresby Plateau (marked with SP in Figure 1b) at around 69.5°N the flow of the shelfbreak EGC separates into two parts; the first continues southwestward along the Greenland shelfbreak and the second part flows toward the Spar Fracture Zone (labeled SPF in Figure 1b). The latter splits again into two different branches on either side of the Kolbeinsey Ridge (labeled KR in Figure 1b). The western part continues toward the Denmark Strait while the eastern part flows to the southeast along the Iceland shelfbreak and likely forms part of overflow east of Iceland. This southward flow along the eastern side of Kolbeinsey Ridge has not been observed. Closer to the Kögur section (KS, blue line in Figure 1b) all of the overflow branches which contribute dense water to the DSOW can be clearly distinguished: the shelfbreak EGC, the separated EGC, and the NIJ. The mean flow field suggests that the separated EGC is fed by a recirculation on the eastern side of the Blosseville Basin (red contour line in Figure 1b) and a portion of the western Kolbeinsey Ridge branch (also confirmed by trajectory analysis, presented later). This recirculation

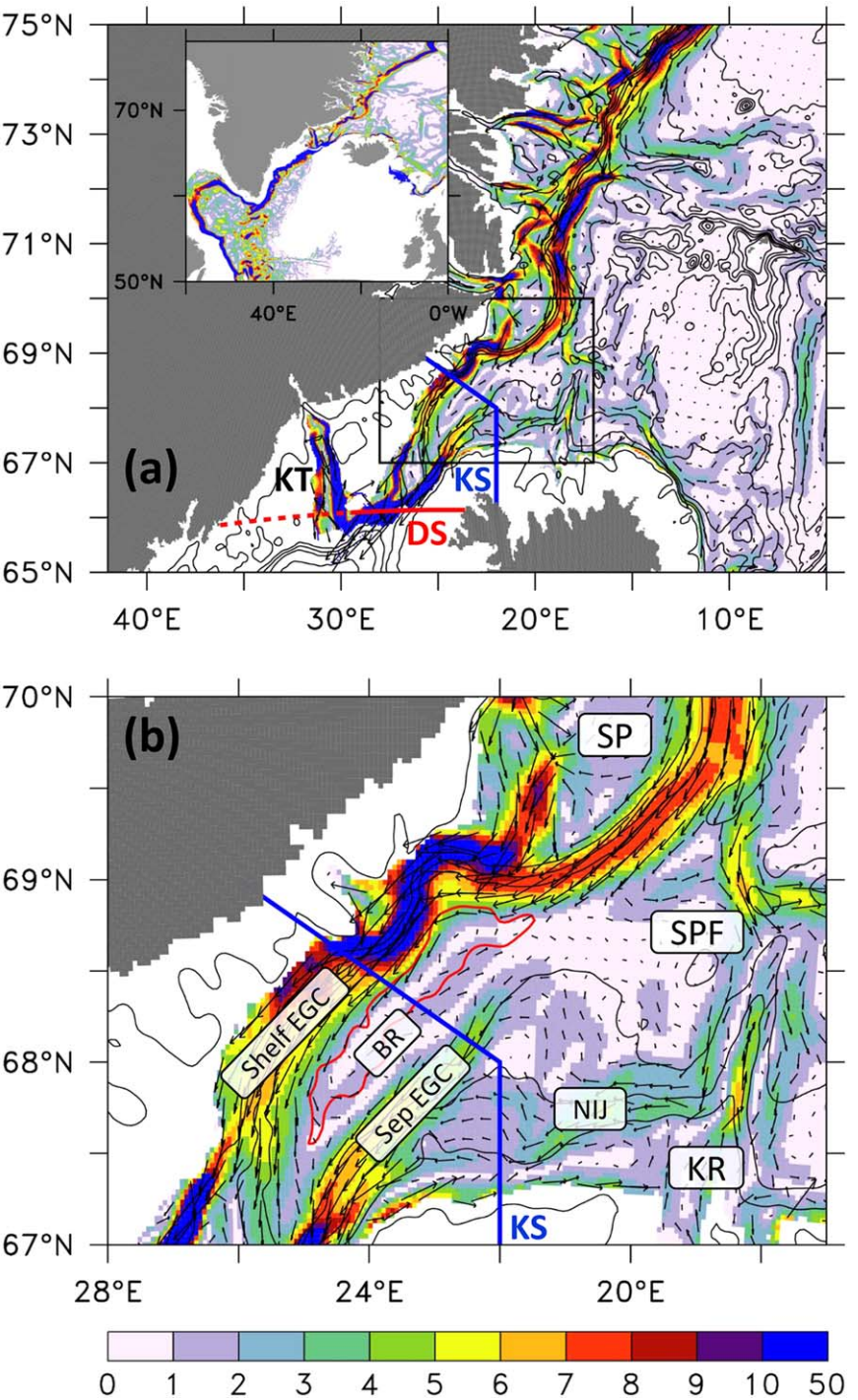

Figure 1. Mean flow speeds (cm/s) on the $\sigma_0 = 28.0$ kg/m^3 isopycnal surface are shown in Figures 1a and 1b over the period 2000–2009. The black box in Figure 1a indicates the zoom region shown in Figure 1b. The inset in Figure 1a illustrates mean flow on $\sigma_0 = 27.9$ kg/m^3 for the North Atlantic region. Black contour lines show model bathymetry contours (250 m interval). Every 10th/4th velocity vector is shown in (a)/(b) and vectors above 5 cm/s are scaled by a factor of 0.05. The red contour line indicates the 1400 m isobath and marks the Blosseville Basin. The Denmark Strait (DS) section is marked in red. The dashed segment of this section marks the Kangerlussuaq Trough region (KT). The Kögur section (KS) is marked in blue and further labeled are the Scoresby plateau (SP), Spar Fracture Zone (SPF), Blosseville Recirculation (BR), the Kolbeinsey Ridge (KR), and the flow branches of the DSOW (shelfbreak East Greenland Current (Shelf EGC), separated East Greenland Current (Sep EGC), and North Icelandic Jet (NIJ)).

in the Blosseville Basin is the main source for the separate EGC in our model. Observations do not support the Kolbeinsey branch as a source for the separated EGC. Studies by *Harden et al*. [2016] and *Våge et al*. [2013] suggested that the near-surface part of the separated EGC is formed by eddies from the shelfbreak EGC, shed at the northern end of the Blosseville Basin. For the deep part, which is presented here, we could not confirm the eddy shedding process and did not find elevated eddy kinetic energy in this region. A possible explanation for this misfit and the lack of eddy shedding might be related to the model bathymetry which might not capture critical details important to eddy shedding. For example, a more abrupt change in the model bathymetry near the Scoresby Plateau would make the shelfbreak EGC more unstable and promote eddy shedding. The model results show a cyclonic gyre circulation where the shelfbreak EGC is the southward branch and the Blosseville Recirculation the northward branch. Observations in this region do not support this cyclonic gyre circulation. As shown later, transports of the overflow shelfbreak EGC are distinctly higher than observations which could be a potential factor affecting this local circulation in the Blosseville Basin and would also point to a too vigorous gyre circulation in the Nordic Seas. Unfortunately, a clear explanation for the discrepancy between observation and model results for the separated EGC remains absent and would require further sensitivity simulations. The NIJ is formed by the combination of the western Kolbeinsey Ridge branch and a return flow of the North Icelandic Irminger Current (NIIC) descending along the Iceland shelf and local water mass transformation east of the Kolbeinsey Ridge (shown in section 3.6). The last two portions describe the dominant sources for the NIJ. This finding provides additional evidence for the hypothesized local overturning loop north of Iceland in a realistic model setup [*Våge et al*., 2011]. South of the Kögur section a part of the shelfbreak EGC, the separated EGC, and the NIJ converge on the eastern side of the Denmark Strait. The remaining part of the shelfbreak EGC stays on the western shelf of the Denmark Strait and crosses the sill together with the eastern branch. South of the sill the flow descends along the Greenland shelf and forms the DWBC, which can be tracked downstream in the Labrador Sea in observations and this model simulation [*Behrens*, 2013; *Fischer et al*., 2015]. We note that large variability (temporally and spatially) in all of these flow branches is present but not reflected in this long-term mean which thus simplifies the circulation, especially north of Iceland.

3.2. Mean Hydrographic Properties Along the Kögur and Denmark Strait Sections

The mean physical properties (temperature, salinity, and cross-section velocity) over the period from 2000 to 2009 across the Kögur and Denmark Strait sections are shown in Figure 2 and are in good agreement with existing observations [*Våge et al*., 2013; *Jochumsen et al*., 2015; *de Steur et al*., 2016; *Harden et al*., 2016; *Mastropole et al*., 2016].

The temperature and salinity signatures across the upper part of the Kögur section (Figures 2a and 2b) show two distinct water masses: in the west cold ($\Theta < -1$°C) and fresh ($S < 34.6$) waters of polar origin carried by the EGC southward and warm ($\Theta > 3$°C) and salty ($S > 34.9$) Atlantic waters in the east associated with the NIIC. The front between these water masses is located around 250 km at this section. We note that the model does capture the subsurface maximum of salinity and temperature of Atlantic origin water in the EGC (seen in *Våge et al*. [2013] and *Harden et al*. [2016]) in the monthly means but not in this 10 year mean. The reason for this behavior is the large temporal variability of the Atlantic core, which is not a persistent feature in our simulation. The cross-section velocities (Figure 2c) show distinct, well-defined flow branches in close agreement with recent measurements [*Våge et al*., 2013; *de Steur et al*., 2016; *Harden et al*., 2016]. In the following, we use the 27.8 kg/m^3 isopycnal to distinguish upper from lower levels. According to the mean velocity field we can define the following branches (Figure 2c): the surface-intensified shelfbreak EGC between 0 and 175 km, the Blosseville Recirculation between 175 and 220 km, the upper separated EGC between 220 and 330 km, the lower separated EGC between 220 and 270 km, the NIJ between 270 km and the Iceland coast, and the NIIC west of 330 km. Since the 27.8 kg/m^3 isopycnal intercepts a small portion of the NIIC, only southward velocities in this region are associated with the NIJ, otherwise they contribute to the NIIC. The horizontal boundaries for our definitions are invariant in time, while the 27.8 kg/m^3 isopycnal shows large vertical variations in time. Variations in the horizontal boundaries do affect the mean transports but have little effect on the variability of individual transport branches.

Across the Denmark Strait section (Figures 2d–2f), polar and subpolar water masses can be identified again on both sides of the section. We note the section follows the model grid for the Lagrangian analysis presented later and thus includes part of the Kangerlussuaq Trough, to the west of the red dashed line in Figures 2d–2f. The Atlantic inflow signature of the NIIC is clearly visible at the Iceland shelfbreak, resulting in

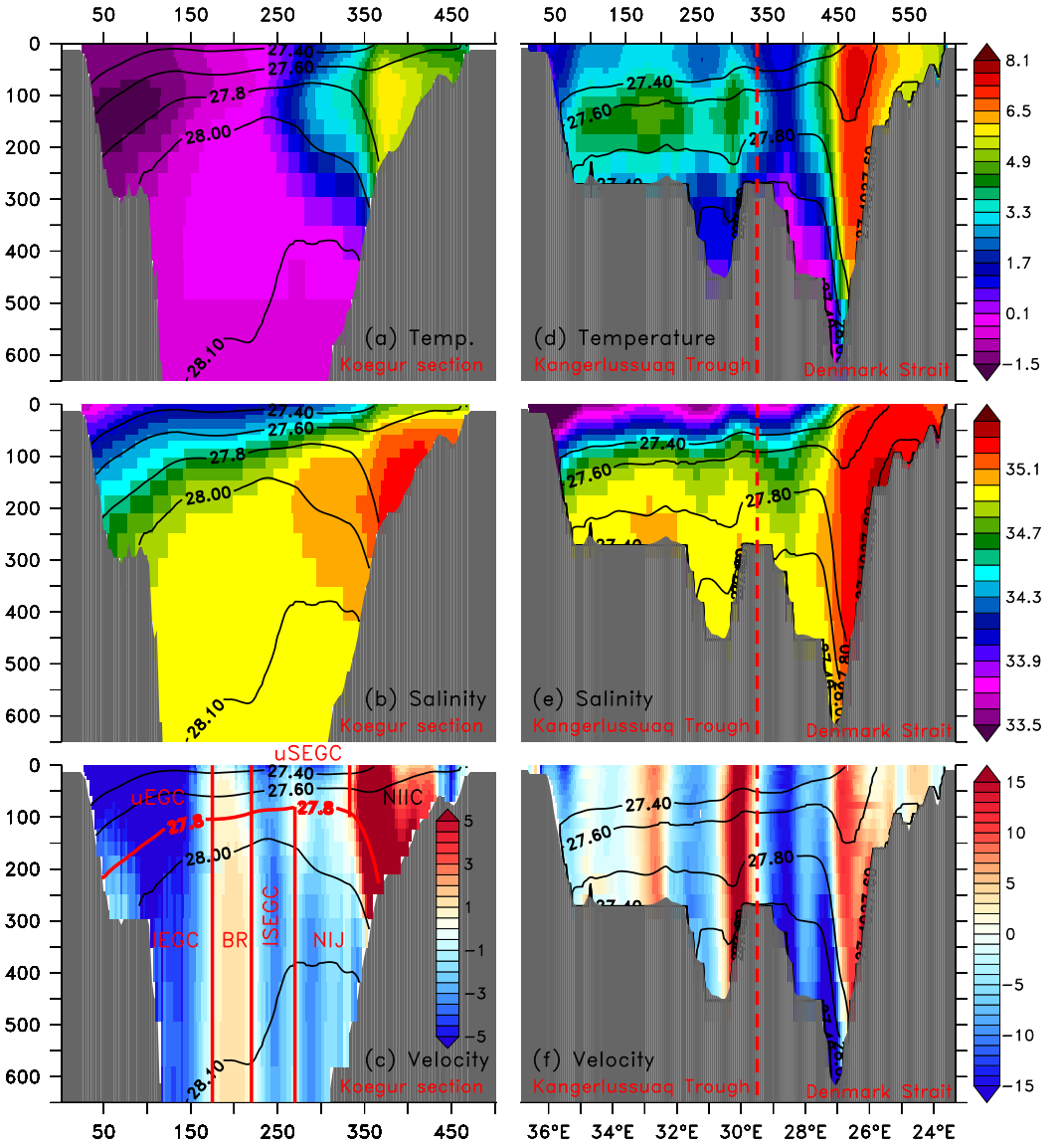

Figure 2. Mean physical properties along the (a–c) Kögur section and (d–f) Denmark Strait section over the period 2000–2009. (a, d) Temperature in °C; (b, e) salinity and (c, f) cross-section velocity in cm/s. Both sections are shown in Figure 1a. Negative velocities indicate southward flow. The *x* axis in Figures 2a–c and 2d represents the distance in km from Greenland coast. Black contour lines show σ_0 contours (kg/m^3). Red labels in Figure 2c refer to certain transport branches: uEGC (upper shelfbreak East Greenland Current), lEGC (lower shelfbreak East Greenland Current), BR (Blosseville Recirculation), uSEGC (upper separated East Greenland Current), lSEGC (lower separated East Greenland Current), NIJ (North Icelandic Jet), and NIIC (North Icelandic Irminger Current). The red contour line in Figure 2c indicates the $\sigma_0 = 27.8$ kg/m^3 isopycnal to differentiate the upper from the lower transport branches. The color scale is the same for Kögur and Denmark Strait section, except for velocity.

the high temperature ($\Theta > 5$°C) and salinity ($S > 35$) signal in this region. To its west two overflow cores can be identified: where the composite core of a portion of the shelfbreak EGC, the separated EGC, and the NIJ occupies the deepest part of the Denmark Strait and the main shelfbreak EGC core is centered around 28.5°W and is visible over the entire water column. In this region, on the western flank of the Denmark Strait and below 300 m, we also find the coldest (~ -1°C) temperature across the Denmark Strait, which is in agreement with recent studies [*Mastropole et al.*, 2016]. The remaining water column has distinctly warmed by around 1°C in comparison to the Kögur section. In the Kangerlussuaq Trough region (left of the red dashed line), we observe a subsurface temperature maximum ($\sim$4°C) which originates from the Irminger Current and is carrying water of subtropical origin in the trough. Additional evidence for this water mass is provided by elevated salinities in this region (Figure 2e). Both cross sections complement the flow field described in Figure 1 and section 4.1.

Table 1. Seasonal Transports[a]

	Vol mean/STD	Vol min	Vol max	FW mean/STD	FW min	FW max
NET	−3.67 ± 1.89	−5.30 [Jan]	−1.94 [Jul]	−39.18 ± 28.94	−69.90 [Nov]	−9.57 [Jun]
Overflow	−3.19 ± 0.82	−3.98 [Mar]	−2.98 [May]	7.95 ± 5.02	3.45 [Apr]	11.23 [Sep]
Shelfbreak EGC	−3.46 ± 1.78 (−2.27 ± 1.13)	−5.22 [Nov]	−1.18 [Jun]	−16.45 ± 15.83	−37.06 [Oct]	−2.28 [May]
Blosseville Recirculation	0.39 ± 0.57	−0.09 [Oct]	−0.01 [Feb]	−2.45 ± 2.32	−4.62 [Nov]	−0.47 [May]
Separated EGC	−1.08 ± 0.48 (−0.90 ± 0.45)	−1.38 [Jun]	−0.82 [Apr]	1.15 ± 2.77	−0.12 [Dec]	2.60 [Jun]
NIJ	(−0.86 ± 0.18)	−0.94 [Apr]	−0.74 [Jan]	4.45 ± 1.22	3.72 [Apr]	4.99 [Jan]
NIIC	1.27 ± 0.62	0.73 [Mar]	1.79 [Aug]	−9.14 ± 6.38	−13.83 [Oct]	−4.45 [Apr]
Sea ice	−0.02 ± 0.01	−0.03 [Mar]	0 [Sep]	−16.81 ± 15.61	−29.66 [Mar]	−1.97 [Aug]

[a]Transport statistics based on climatological means across the Kögur section. The climatology is constructed over the period 1960–2009 over the entire water column. Overflow is water denser than 27.8 kg/m^3 and above 650 m (sill depth of the Denmark Strait). Volume transports in round parentheses represent transports of water denser than 27.8 kg/m^3. Volume transports are given in Sv (negative values indicate a southward flow), freshwater transports (S_{ref} = 34.8) in mSv (negative values indicate a southward freshwater transport). Square brackets show the month of occurrence. Standard deviations for the volume and freshwater transport are based on monthly means.

3.3. Long-Term Mean Transports Across the Kögur Section and the Denmark Strait

The well-distinguishable flow branches across the Kögur section (Figure 2c) allow the computation of volume and freshwater transports for each individual branch and the investigation of their variability. The mean full-depth net and overflow ($\sigma_0 > 27.8$ kg/m^3) transports across the Kögur section over the period (1960–2009) sum up to −3.7 and −3.2 Sv, respectively (see also Table 1). *Harden et al*. [2016] estimated the overflow transport to be −3.5 ± 0.16 Sv from 1 year-long mooring time series, which is in good agreement with the simulated overflow transport. Considering only transports above the sill depth of Denmark Strait (>650 m) the simulated transport reduces to −3.2 Sv and provides a similar aspiration rate as the observations of about −0.5 Sv [*Harden et al*., 2016].

The simulated full-depth mean transports for the individual flow branches are: shelfbreak EGC −3.5 Sv, separated EGC −1.1 Sv, and NIJ −0.86 Sv. Transports for the northward flowing branches are: NIIC 1.3 Sv and BR 0.4 Sv. The overflow transports ($\sigma_0 > 27.8$ kg/m^3) for the shelfbreak and separated EGC are −2.3 and −0.9 Sv, respectively (Table 1). Observations for the overflow branches suggest values for the shelfbreak and separated EGC and NIJ are −1.5, −1, and −1 Sv, respectively [*Harden et al*., 2016]. The simulated overflow transports of the separated EGC and the NIJ roughly agree with the observational values. The transport values of the modeled shelfbreak EGC are around 0.5 Sv higher than the observations, even when taking the Blosseville Recirculation into account. The reasons for this discrepancy remain unclear.

For the Denmark Strait, the simulated full-depth mean net transports are −3.7 and −3.8 Sv ($\sigma_0 > 27.8$ kg/m^3) for the period 1960 to 2009. We recognize a 15% increase in the overflow transport compared to the Kögur section of about ∼0.6 Sv potentially due to water mass transformation, convection as part of the NIJ overturning loop and/or mixing of dense overflow with lighter water masses. The overflow component in the Denmark Strait is slightly higher than the long-term mean of 3.4 Sv [*Jochumsen et al*., 2012] obtained over the period 1996–2011. The simulated overflow transport for this period (1996–2009) is 3.71 Sv and similar to the long-term mean.

The mean net freshwater transport across the Kögur section sums up to −39.2 mSv, where sea ice is responsible for about ∼40% of the freshwater transport (see also Table 1). Our net (liquid and solid) freshwater transports are distinctly lower than the values (liquid) obtained by *Våge et al*. [2013] and *de Steur et al*. [2016] of about −159 and −65 mSv, respectively. The reasons for this large mismatch are likely related to a positive salt bias in the Nordic Seas in this simulation [*Behrens*, 2013], which offsets the mean values, but does not have much of an effect on the variability of freshwater transport which is highly linked to transport variations. Nevertheless, current observations also provide evidence for large variations of the freshwater transport between individual months [*de Steur et al*., 2016].

The mean northward heat transport across the Kögur section sums up to 35.7 TW relative to 0°C, which agrees with the value provided by *Köhl et al*. [2007] of about 40 TW based on an assimilation product.

3.4. Seasonal Transport Variability Across the Kögur Section

The climatological monthly transports in this sections are based on 50 years over the period 1960–2009 (Figure 3). A clear seasonal signal is present in all transport branches (upper and lower parts combined),

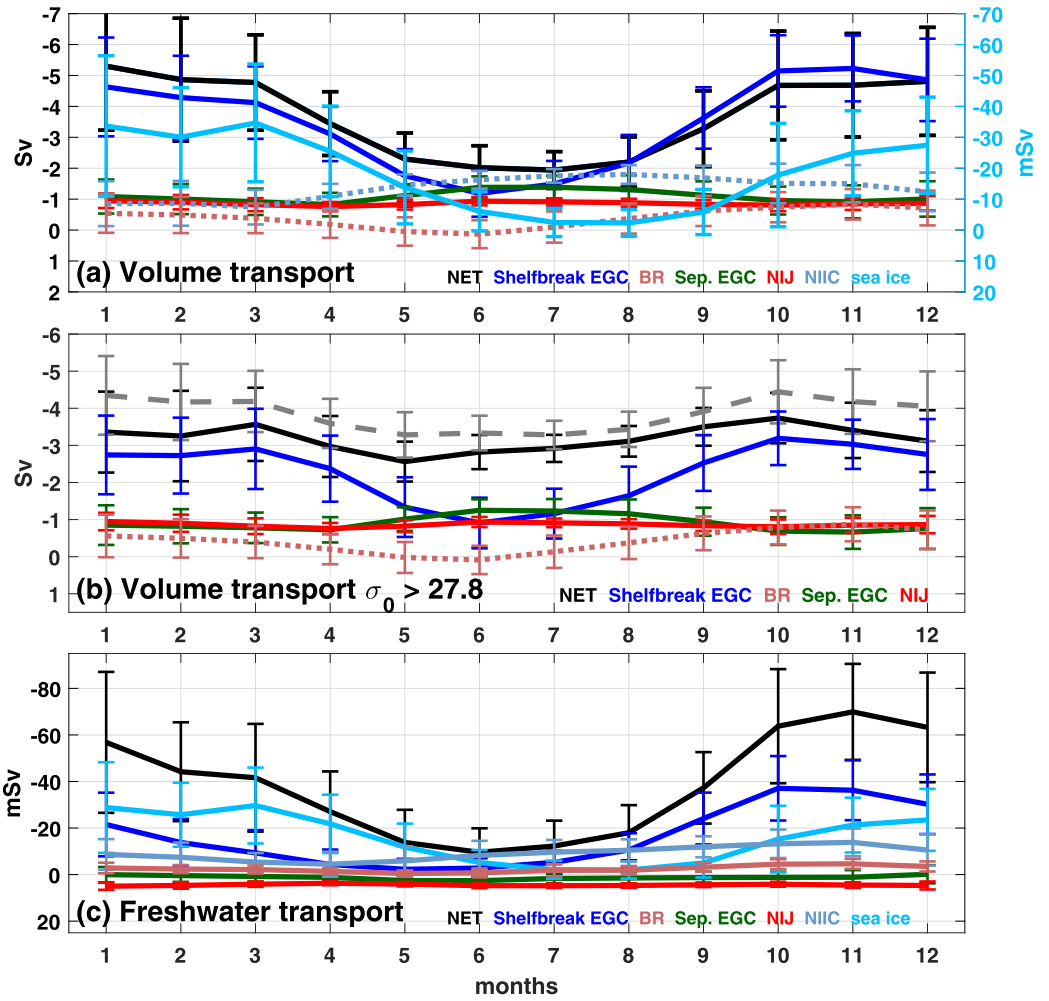

Figure 3. Seasonal cycle of full depth transports across the Kögur section for the period from 1960 to 2009 constructed from monthly means; (a) volume transports (in Sv) and sea ice (in mSv, right scale); dotted lines represent positive/northward transports (b) volume transports for overflow water ($\sigma_0 > 27.8$ kg/m^3) (in Sv), grey dashed curve represents the transport across the Denmark Strait; dotted lines represent positive/northward transports (c) freshwater transports (in mSv (10^3 m^3/s), Sref = 34.8); (negative values indicate a southward transport, see also Table 1, for mean/min/max values). Error bars show the standard deviation.

which contribute to the DSOW (Figure 3a). The net, the shelfbreak EGC, and the volumetric sea ice transport show lower transports during the summer months (May to September) and enhanced southward transports during the winter months (October to March) (see also Table 1). The separated EGC is characterized by an opposite behavior with a slightly enhanced southward flow during the summer months (May to September). However, the seasonal variations are small compared to the variability present in the shelfbreak EGC, which varies around 2 Sv on a seasonal time scale and is in good agreement with *Jónsson* [1999]. Transports of the NIJ are fairly constant and do not show a significant seasonal cycle. The transport of the Blosseville Recirculation is enhanced during winter and weak during the summer months. Its northward transport compensates to some extent the enhanced transports of the shelfbreak EGC during the winter season. The opposing phases between the shelfbreak EGC and the separated EGC have also been found in the mooring data of *Harden et al.* [2016] and can be linked to local winds. The general northward transport of the NIIC is enhanced from April to December with a peak in July, which is consistent with observations [*Jonsson and Valdimarsson*, 2012]. The volumetric transport of sea ice peaks in March and decreases until August, when its minimum and lowest sea ice cover are reached. The large standard deviations indicate large variability, especially in the shelfbreak EGC and sea ice. However, the described seasonal signals are significant (greater than the standard deviation).

We note that most of the seasonal signal is closely linked with transports within the upper branches, and the seasonal cycle is distinctly reduced in the deeper branches ($\sigma_0 > 27.8$ kg/m^3, Figure 3b). The net transport across Kögur and Denmark Strait (grey dashed line) shows one significant transport maximum in October. The transport maxima are connected to the seasonal cycle of the shelfbreak EGC showing the same seasonality. The larger net transports in the Denmark Strait compared to the Kögur section points to water mass transformation possibly by convection or mixing of denser with lighter overflow water in this region. Since the difference is largest during the winter months (October to March) it suggests that convection during this period is the more likely reason. The weak seasonal cycle of the separated EGC and NIJ transport does compensate the weaker shelfbreak transports during the summer month to some extent. We note that observations do not show any pronounced seasonal modulation of the overflow in Denmark Strait [*Jochumsen et al*., 2012], which points to shortcomings in the model results and/or in the atmospheric forcing data. This misfit needs further attention but is beyond the scope of this study.

The net southward freshwater transport (solid black, $S_{ref} = 34.8$) shows a seasonal cycle similar to the net volume transport ($r = 0.93$). The largest export of freshwater from the Nordic Seas to the south occurs during the early winter months, with a peak in November (Figure 3c), about 1 month delay relative to Fram Strait (not shown). The lowest freshwater transport is reached in June coherent with the Fram Strait. The largest contributors to the net freshwater transport are the shelfbreak EGC and sea ice. Observations suggest that, for the liquid freshwater content, around 70% are carried by the shelfbreak EGC and 30% by the separated EGC to the south [*de Steur et al*., 2016]. The model results agree with a 70% contribution of the shelfbreak EGC, but show no significant contribution of the separated EGC to the freshwater budget, maybe due to the positive salt bias in this simulation. The seasonal cycle of the shelfbreak EGC and sea ice are quite similar during the first half of the year, but the contribution of the shelfbreak EGC ramps up faster than the sea ice and peaks in October, whereby the freshwater transport of sea ice slowly increases and peaks in March. Observation of sea ice transport across the Fram Strait also suggest a peak in March [*Vinje*, 2001]. The contributions of the separated EGC, the Blosseville Recirculation, and the NIJ to the net freshwater transport across the Kögur section are negligible (see Table 1). This is in contrast to observations, where the separated EGC contributes a significant portion to the net freshwater transport. The positive sign of the NIJ indicates that it transports freshwater northward by exporting salt to the south. In general, the variability of the freshwater transport is dictated by the variability of the volumetric transport but also, to some extent, by the seasonal cycle of the coastal runoff from Greenland and sea ice melt, which is enhanced during the summer months [*Bamber et al*., 2012].

3.5. Interannual Transport Variability Across the Kögur Section

In the following section, we assess the variability of these flow branches on interannual and longer time scales. None of the branches show a distinct long-term transport trend over the simulation period from 1960 to 2009 (Figure 4a). This finding is in line with observations in the Denmark Strait [*Jochumsen et al*., 2012, 2015], which also do not show any long-term trend in the overflow.

The shelfbreak EGC has the largest year to year transport variability with a range from -2.25 to -4.72 Sv in these annual averages, while the transports of the separated EGC and NIJ are rather constant and do not show much year to year fluctuations (see Table 2). The separated EGC does, however, show some long-term modulations (enhanced transports are present for periods between 1970–1990, 1995–2000, and from 2005 onward) opposing the variability of the shelfbreak EGC. This negative relation between both EGC branches is also present on seasonal time scales and confirms previous findings [*Köhl et al*., 2007; *Harden et al*., 2016]. Substantially lower transport periods (by about 1 Sv) of the shelfbreak EGC and, thus, in net transport, occur during 1975–1978, 1983–1988, 2000–2003 and larger transports during 1967 and 2005. Variability of the net, shelfbreak and sea ice transports are highly linked to the large-scale atmospheric conditions, in particular, to the wind stress curl south of Iceland, indicated by the grey shaded area (Figure 4a). Correlation coefficients between net transports and wind stress curl for the annual means are shown in supporting information Figure S1a and reach up to 0.8 south of Iceland for the 50 year long record. Although the wind stress curl south of Iceland is related to the NAO ($r = 0.43$, supporting information Figure S2b/c), no direct link between transport variability of net or overflow transports and NAO index can be found in Denmark Strait or across the Kögur section (supporting information Figures S2d and S2e). The correlations between net and overflow transports are 0.86 and 0.77 for the Denmark Strait and Kögur sections respectively, suggesting a reduced influence of wind stress anomalies on the overflow transport variability (supporting information Figure S2d and S2e) while overflow transports between Kögur and

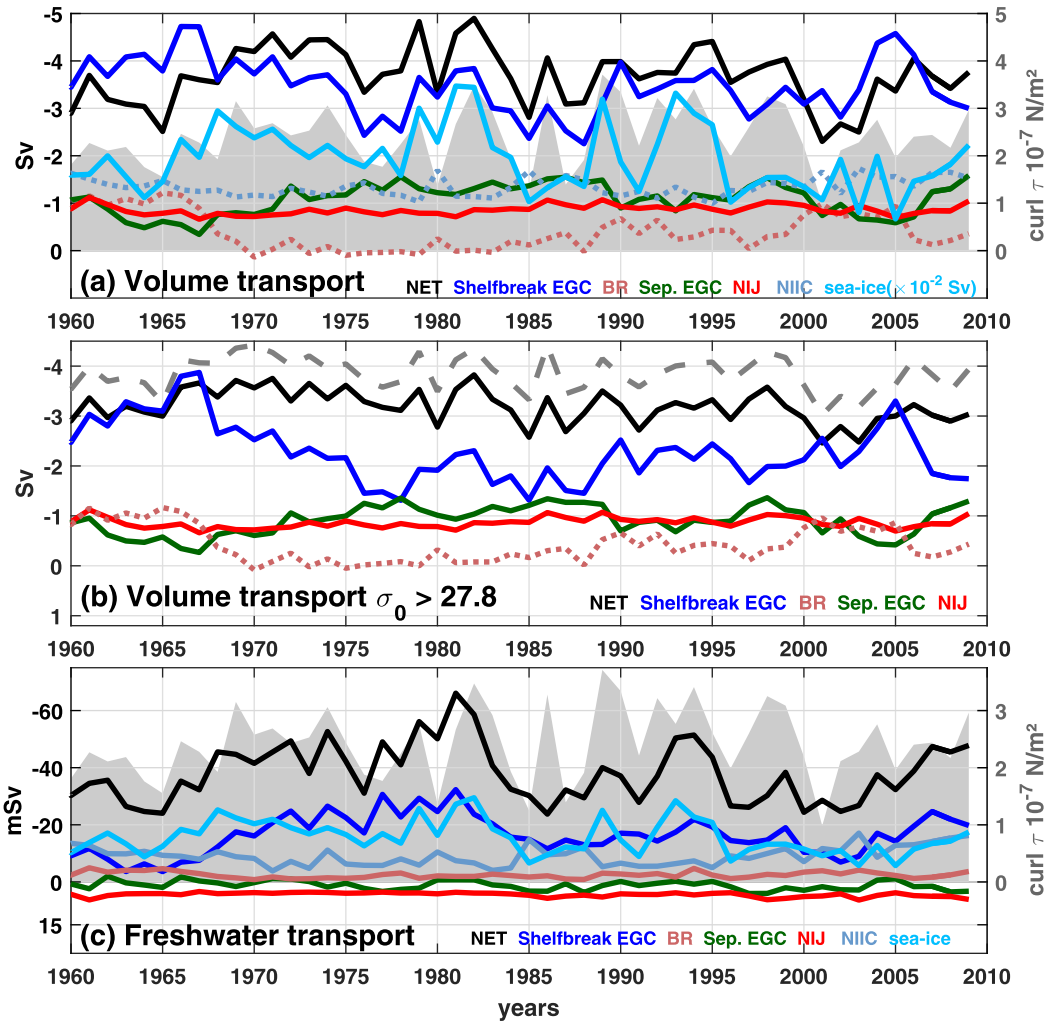

Figure 4. Annual full-depth mean transports across the Kögur section for the period from 1960 to 2009; (a) volume-metric transports (left scale in Sv), grey shaded area shows annual mean wind stress curl (10^{-7} N/m^2) averaged over a region south of Iceland (see supporting information Figure S1); dotted lines represent positive/northward transports (b) volume transports overflow water ($\sigma_0 > 27.8$ kg/m^3, in Sv), grey dashed curve represents the transport through Denmark Strait; dotted lines represent positive/northward transports (c) freshwater transports over the entire water column (in mSv (10^3 m^3/s), Sref = 34.8); (negative values indicated a southward transport, see also Table 2, for mean/min/max values).

Denmark Strait are highly linked (supporting information Figure S2a). Earlier studies show that, for negative NAO events, no clear relation between NAO and overflow in the Denmark Strait are found [*Jochumsen et al.*, 2012] and that transport variability is dictated by local wind forcing [*Harden et al.*, 2016]. However, our results show that the NAO has an impact on the wind stress curl south of Iceland, although it is limited.

As shown in supporting information Figure S1a, the Nordic Seas are mainly characterized by positive wind stress curl and a negative correlation with the net transport across the Kögur section for most of this region (supporting information Figure S1b). The negative wind stress curl along the coast of Greenland is caused by barrier winds [*Våge et al.*, 2013]. The general negative correlation suggests that an increase in wind stress curl over the Nordic Seas causes an enhanced southward transport across the Kögur section. This can be explained by the speed up of the large-scale cyclonic circulation in the Nordic Seas and thus the boundary currents and causes the good match between the variability of the volume transports of the shelfbreak EGC and sea ice with the wind stress curl south of Iceland (r = 0.53). We chose this region due to the highest correlation with the transport, but note that any larger region in the Nordic Seas would show a similar signal to the wind stress curl south of Iceland, since they are not independent. The transports of the Blosseville Recirculation, the NIJ, and the NIIC do not show any clear wind related response, although the transports of the

Table 2. Interannual Transports[a]

	Vol mean/STD	Vol min	Vol max	FW mean/STD	FW min	FW max
NET	−3.67 ± 0.61	−4.89 [1983]	−2.30 [2001]	−39.18 ± 9.76	−58.59 [1982]	−24.04 [1965]
Overflow	−3.19 ± 0.33	−3.82 [1982]	−2.46 [2002]	7.95 ± 1.94	4.93 [2005]	11.90 [1997]
Shelfbreak EGC	−3.46 ± 0.58 (−2.27 ± 0.59)	−4.72 [1976]	−2.25 [1988]	−16.45 ± 6.78	−32.32 [1981]	−3.61 [1965]
Blosseville Recirculation	0.39 ± 0.39	0.13 [1971]	1.21 [1966]	−2.45 ± 1.07	−4.94 [1962]	−0.81 [1970]
Separated EGC	−1.08 ± 0.32 (−0.90 ± 0.29)	−1.58 [2009]	−0.34 [1988]	1.15 ± 1.59	−1.76 [1966]	4.04 [1997]
NIJ	(−0.86 ± 0.10)	−1.12 [1962]	−0.66 [1968]	4.45 ± 0.76	3.68 [1974]	6.34 [2003]
NIIC	1.27 ± 0.19	1.09 [1970]	2.30 [1981]	−9.14 ± 3.31	−17.09 [2003]	−4.03 [1983]
Sea ice	−0.02 ± 0.01	−0.03 [1982]	−0.00 [2004]	−16.81 ± 5.84	−29.71 [1981]	−5.72 [2005]

[a]Transport statistics based on annual means across the Kögur section over the period 1960–2009 over the entire water column. Overflow characterizes water denser than 27.8 kg/m^3 and above 650 m (sill depth of the Denmark Strait). Volume transports in round parentheses represent transports of water denser than 27.8 kg/m^3. Volume transports are in Sv (negative values indicate a southward flow), freshwater transports (S_{ref} = 34.8) in mSv (negative values indicate a southward freshwater transport). Numbers in square brackets show the year of occurrence. Standard deviations for the volume and freshwater transport are based on yearly means.

Blosseville Recirculation and the NIIC show some long-term modulations. Studies by *Våge et al.* [2013] hypothesized that the negative wind stress curl over the Blosseville Basin may result in an anticyclonic gyre circulation. Our results show a cyclonic gyre circulation instead, where the shelfbreak EGC is the southward branch and the Blosseville Recirculation the northward branch. No influence of the wind stress curl or variability of the separated EGC on the Blosseville Recirculation, as seen on seasonal time scales, can be found on interannual time scales.

The year to year fluctuations in the dense overflow branches ($\sigma_0 > 27.8$ kg/m^3, Figure 4b) are considerably smaller than in the surface layer. The shelfbreak EGC shows a remarkable long-term drop from 1965 to 1975 of nearly 2 Sv. The reasons for this substantial decline remain unclear but do not have a large impact on the net transport, which is compensated by enhanced transport of the separated EGC and declining northward transports by the Blosseville Recirculation. In the overflow branches, the opposing tendency of shelfbreak and separated EGC is more obvious ($r = -0.88$) compared to the same calculation with the inclusion of the surface layer ($r = -0.78$). The model results also suggest a close co-variability between net transports at the Kögur section (solid black line in Figure 4b) and across the Denmark Strait (dashed grey line in Figure 4b, see also supporting information Figure S2a), while the Denmark Strait transports are about 0.5 Sv larger, due to the reasons described above.

The net southward freshwater transport (Figure 4c) is, as for the seasonal transports, dominated by the shelfbreak EGC (40%) and the sea ice (40%). The contribution of the other transport branches to the net transport is marginal. The mean freshwater transports of about −39.2 mSv are substantially lower than those reported by *de Steur et al.* [2016], of about 65 mSv (2011–2012). As previously discussed, the difference can, in part, be explained by a positive salinity bias of the model. The net freshwater transport anomalies are strongly linked to the local wind stress forcing (grey shaded areas) and highlights the dynamic response due to changes in the transports rather than changes in salinity itself. It is therefore not surprising to see a general covariability between the freshwater transports of the shelfbreak EGC and sea ice ($r = 0.52$). Periods with increased freshwater export from the Nordic Seas to the subpolar North Atlantic occur between 1968–1975, 1978–1982, 1992–1995, and from 2005 onward, in phase with the large-scale wind forcing. Those freshwater peaks can also be seen in enhanced freshwater transport from the Arctic through the Fram Strait [*Haak*, 2003; *de Steur et al.*, 2009], surface salinity anomalies and in other hydrographic sections in the subpolar North Atlantic [*Dickson et al.*, 1988; *Belkin et al.*, 1998; *Belkin*, 2004], which were termed great salinity anomalies.

In summary, we see a close link between net volume transport and freshwater transport across the Kögur section which is mainly affected by the local wind stress curl pattern but also influenced by the large-scale atmospheric circulation associated with the North Atlantic Oscillation. However, a clear and consistent link to the NAO remains absent. In addition, we observe that volume transports of the shelfbreak and the separated EGC oppose each other.

3.6. Particle Pathways of Overflow Water in the Nordic Seas

In the following section, we investigate the upstream pathways of the densest portion of the DSOW ($\sigma_0 > 28.0$ kg/m^3). The downstream pathways have already been investigated intensively by previous

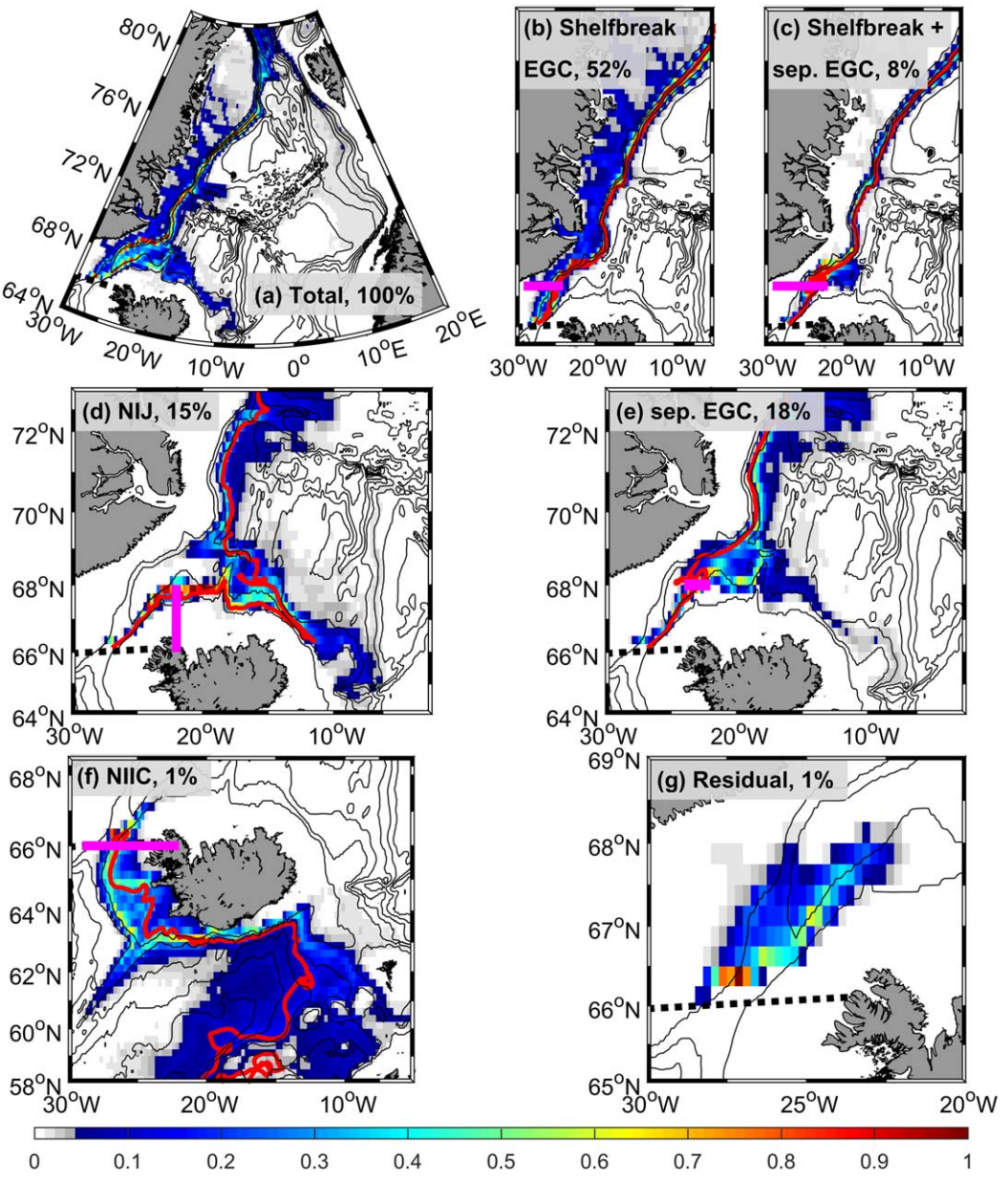

Figure 5. Upstream DSOW pathways: probability density of particles continuously seeded in the Denmark Strait with $\sigma_0 > 28.0$ kg/m^3 and back-tracked, east of 29.5°W over 10 years (2000–2009) and regridded on a regular 0.25° × 0.25° grid (total number of particles seeded: 437,206). Recirculations are not considered. Example trajectories are shown in red. (a) All floats; (b) floats associated with the shelfbreak EGC crossing 68°N from the south between 29°W and 24°W (pink line, 219,792 particles), (c) floats considered as separated and shelfbreak EGC crossing 68°N between 24°W and 22°W and afterward 68°N between 29°W and 24°W from the south (pink line, 34,765 particles), (d) floats considered as NIJ crossing 22°W between 66°N and 68°N from the west (pink line, 65,677 particles), (e) floats considered as separated EGC crossing 68°N between 24°W and 22°W from the south (pink line, 76,079 particles), (f) floats considered as North Icelandic Irminger Current (NIIC) crossing 66°N between 29°W and 22°W from the north (pink line, 3069 particles). (g) Residual floats which have not crossed a section during its life time (6798 particles). Probability density has been scaled to 1. Pink lines mark the control sections. Black contours show the bathymetry (contour interval 500 m).

studies [*Koszalka et al.*, 2013; *von Appen et al.*, 2014]. Lagrangian particles have been continuously seeded across the Denmark Strait section (dashed black line in Figure 5) over a time span of 10 years (437,206 particles in total), and calculated backward in time (see section 2 for details). The obtained probability densities (Figure 5) reveal well-defined flow pathways of the overflow branches upstream of the Denmark Strait.

From the probability density of all particles (Figure 5a), two distinct pathways can be identified: a branch associated with the shelfbreak of Greenland and a branch with the shelfbreak north of Iceland. Particles

following the shelfbreak of Greenland either have Polar origin or are Atlantic-origin water as part of the large-scale circulation in the Nordic Seas. Based on the crossings of certain segments (pink lines in Figures 5b–5f) of the Kögur section, we separate the particles and their origins further (Figures 5b–5g), guided by the transport diagnostics presented above. From the total number of particles, 52% originated from the shelfbreak EGC (crossed 68°N between 29°W and 24°W), 15% from the NIJ (crossed 22°W between 66°N and 68°N), 18% from the separated EGC (crossed 68° between 24°W and 22°W), 1% from the NIIC (crossed 66°N between 29°W and 22°W), and 1% residual particles which did not reach any section. Note that the particle density does not reflect any volumetric contribution to the DSOW. We also found particles which crossed multiple sections, or the same section several times (see also supporting information Figure S3 and Table S1). A common combination being particles contributing to both branches of the EGC as part of the Blosseville Recirculation (8%). Most particles can be identified as shelfbreak EGC (Figure 5b) following the coast of Greenland. The model results also suggest that some of these particles originate from fresh on-shelf waters or Greenland fjords, even though they were all seeded in the densest portion of the DSOW ($\sigma_0 > 28.0$ kg/m^3). If particles recirculate in the Blosseville Recirculation and enter the shelfbreak EGC, then they show generally less on-shelf contribution then shelfbreak-only floats (Figure 5c). Particles associated with the NIJ (Figure 5d) follow the northern Iceland shelfbreak. East of the Kolbeinsey Ridge a portion turns northward and follows the shelfbreak of Greenland, while a smaller portion seems to originate from further east of Iceland. These latter particle trajectories provide additional evidence for the hypothesized downwelling of water along the Iceland slope [*Våge et al.*, 2011]. The separated EGC (Figure 5e) shows a preference for a more northern flow path compared to the NIJ and only a small fraction crosses the Kolbeinsey Ridge. In addition, the branch along the Kolbeinsey Ridge is preferred but, in addition, particles follow a western branch close to the Greenland shelf as well, such as those illustrated with the example trajectory. The trajectories also suggest that a small fraction of NIIC waters originating from south of the Iceland Scotland Ridge recirculates directly into the DSOW (Figure 5f) and a small portion does not reach any of these sections within 10 years (Figure 5g). These trajectory-based results are in line with the long-term mean flow field presented in Figure 1.

In the following analysis, we use temperature and salinity of each particle to map their location and thus the probability density into Θ-S space (see Figure 6 and section 2). The temperature and salinity of initially seeded particles varied between roughly −1°C to 3°C and 34.75 to 35.15 (indicated by the red dashed box in Figures 6a–6c). The density of these particles varied between 28.0 and 28.1 kg/m^3, close to the observations, which show a maximum density of about 28.1 kg/m^3 at the Denmark Strait sill [*Macrander et al.*, 2007]. Over the course of the 10 year long seeding period backward in time the temperature and salinity properties might change from their initial values, and provide additional insights about the sources of the DSOW and water mass transformation (Figure 6b). However, the highest probabilities are still found within similar initial Θ-S overflow properties (dashed box in Figure 6b), and a maximum in this space is centered at −0.5°C and 34.95. That indicates that a large number of particles (60%) do not change their temperature and salinity properties much over the 10 year period. Their geographical probability density is shown in Figure 6d for those particles with Θ-S properties within the initial Θ-S range over the 10 year period. They mainly originate from north of the Fram Strait and can be found north of Iceland and mainly along the shelfbreak of Iceland. Apart from this main contribution, two different sources can be identified with lower and higher salinities compared to the initial values.

One branch is characterized by generally lower temperatures and distinctly lower salinities, which nearly reaches freezing temperature of around −2°C and salinity of 33.5. Based on these properties it reflects fresh and cold coastal waters from Greenland, which is confirmed by the geographical probability density of those particles with salinities reaching less than 34.75 (27.5% of all particles, Figure 6e). This shelf water has a Polar origin and is transported within the EGC system toward the Denmark Strait. On its way south, its density increases toward overflow densities due to local air-sea fluxes, sea ice interactions (heat loss, seasonal brine rejection due to see ice growth) and mixing with Atlantic origin water [*Rudels et al.*, 2002]. A signature of this very cold (∼−1°C) water mass can be seen on the western flank of the Denmark Strait section (Figure 2d).

The second source branch shows temperatures between 3°C and 12°C and a salinity around 35.25, which indicates waters with Atlantic origin south of the Greenland-Scotland Ridge (12.5%). The geographic probability (Figure 6f) suggests that this water is a combination of Atlantic water associated with a fraction of direct inflow facilitated by the NIIC entering through Denmark Strait and Atlantic-origin water as part of the

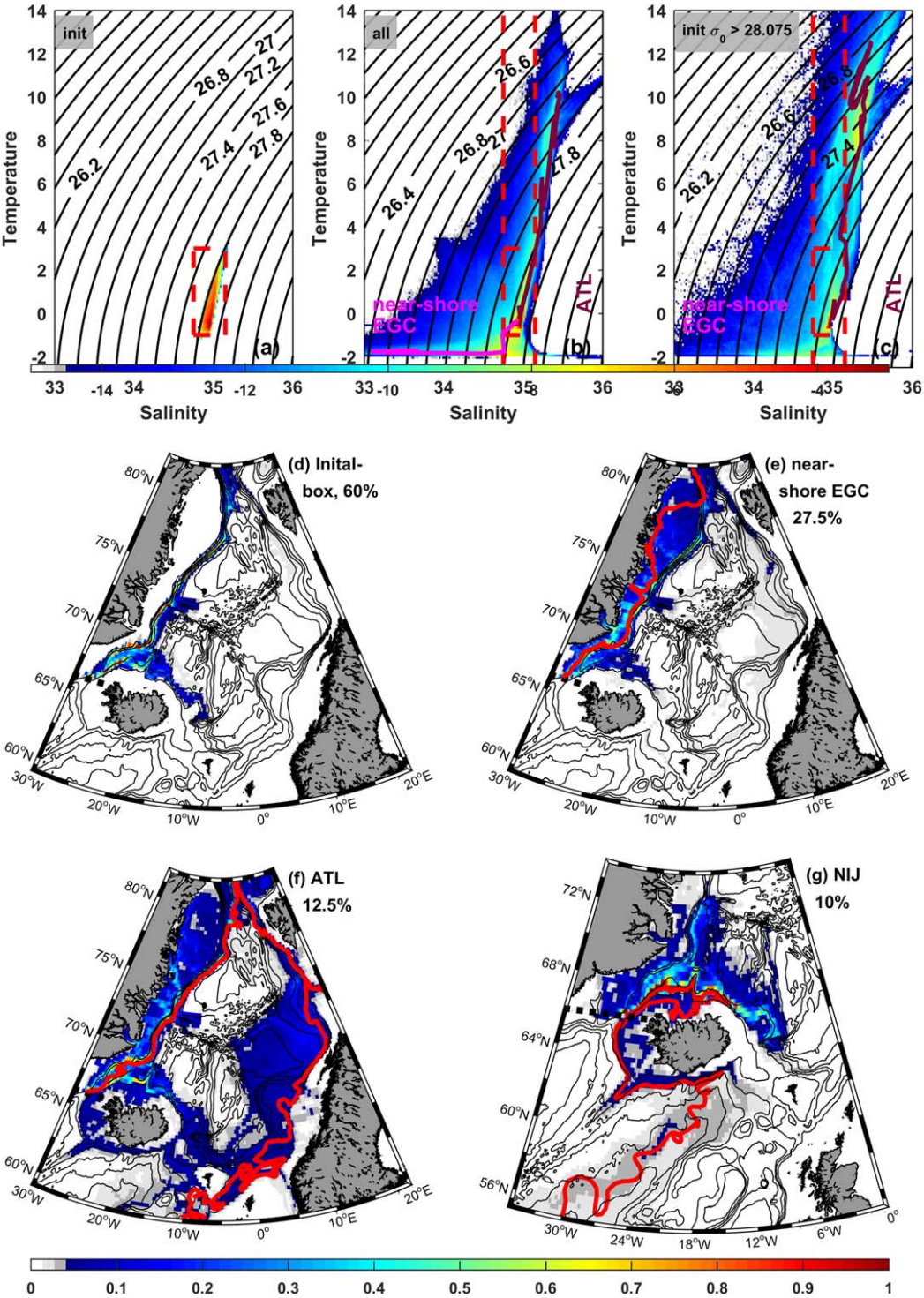

Figure 6. Probability density in the Θ-S space of particles seeded in the Denmark Strait (as described in Figure 5). (a) Initial seeding probability density along the Denmark Strait section. (b) Time mean probability density of backward tracked particles. The red dashed lines are for guidance of the initial release probability density. (c) Same as Figure 6b but for particles with initial densities (σ_0) larger than 28.075 kg/m^3 contributing to the densest part of the DSOW. Temperature and salinity evolution are provided for some exemplary trajectories (magenta and dark red), which have some Arctic (fresh) and subtropical North Atlantic (salty) origin. The probability for Figures 6a–6c sums up 1 each, and the scale logarithmic. (d) Geographical probability of particles staying within the initial Θ-S range (118,305 particles) defined by $34.75 > S > 35.1$ and $-1°C > \Theta > 3°C$ and (e) particles reaching salinity < 34.75 (51,918 particles) and (f) particles reaching salinity > 35.1 (51,918 particles) during their lifetime. (g) Particles with initial densities (σ_0) larger than 28.075 kg/m^3 and not reaching not latitudes of 75°N (66,972 particles). Red lines show the particle trajectories from Figures 6b and 6c. The total amount of seeded particles are 437,206. The summed probability in Figures 6d–6g are scaled to 1. Recirculating particles are not considered. Black contour lines show the bathymetry (contour interval 500 m).

cyclonic circulation in the Nordic Sea which mainly originates from the Atlantic inflow into the Nordic Seas through the Faroe-Shetland channel. This Atlantic Water follows the Norwegian shelfbreak toward the Fram Strait before it returns along the Greenland shelfbreak south toward the Denmark Strait as Atlantic—origin overflow water [*Mauritzen*, 1996]. Along its way it loses heat which makes it less buoyant (see particle trajectory in Θ-S space, Figure 6b) contrary to the near shore EGC trajectory which increases in salinity to become denser. If we now just focus on the densest part of the DSOW with initial $\sigma_0 > 28.075$ kg/m^3 and thus associated with the NIJ (Figures 6c/6g) we see in Θ-S space that probabilities increase toward particles with Atlantic origin compared to probabilities of all particles (Figure 6b). That is also demonstrated in the geographical distribution (Figure 6g) which shows the highest particle probabilities along the northern Iceland shelf and toward the Iceland Sea, for particles which have their origin south of Denmark Strait, as illustrated by the example trajectory. This trajectory is carried with the Irminger Current toward the Denmark Strait and travels within the NIIC along the Iceland shelf to the east before it downwells east of the Kolbeinsey Ridge. At that point, it changes direction and is carried within the NIJ toward the Denmark Strait and thus completes the overturning loop that involves the boundary current system north of Iceland and water mass transformation in the Iceland Sea hypothesized by *Våge et al*. [2013]. Despite this general agreement, there is one inconsistency which needs further attention. *Våge et al*. [2011, 2015] found that the wintertime densification occurs primarily in the interior Iceland Sea and concluded that this region is a main source for the NIJ. The model results, on the other hand, indicate that most of the water mass transformation takes place within the NIIC. The reasons for this discrepancy remain unclear but could be related to deficiencies in the atmospheric forcing.

4. Conclusions

Our results show that a high-resolution model configuration (VIKING20) is able to simulate the local conditions in the Denmark Strait and north of Iceland with high realism. This is mainly achieved by the fine model mesh, which allows explicit resolution of mesoscale features and the complex current system [*Behrens*, 2013; *Böning et al*., 2016].

Simulated hydrographic properties and velocities across the Kögur section north of the Denmark Strait compare well with the hydrographic measurements reported in recent studies [*Våge et al*., 2013; *de Steur et al*., 2016; *Harden et al*., 2016]. The model does particularly well in resolving all of the different transport branches contributing to the DSOW: the shelfbreak EGC, the separated EGC, and the NIJ. Disagreements between the model and observations exist for the origin of the separated EGC which needs further investigation. The simulated seasonal variability of the net transport across the Kögur section, which shows reduced southward transports during summer, is dominated by the seasonal cycle of the shelfbreak EGC. The separated EGC and the NIJ show an opposite seasonal cycle to the shelfbreak EGC and compensate the shelfbreak variability to some extent. This anticorrelation between the shelfbreak and the separated EGC is also found on interannual time scales. The simulated overflow transports ($\sigma_0 > 27.8$ kg/m^3) for the separated EGC and NIJ, -1.1 and -0.86 Sv, respectively, agree well with the observed transports of about -1 Sv for each branch [*Harden et al*., 2016]. The simulated transports of the shelfbreak EGC are roughly 0.5 Sv higher than the observations (-1.5 Sv) [*Harden et al*., 2016]. The observations and model results agree that the shelfbreak EGC contributes the largest fraction to the DSOW, while the NIJ supplies the densest water.

The net freshwater export to the south, which is dominated by the shelfbreak EGC and sea ice, is reduced during summer but increases during autumn, as soon as the southward transport of the shelfbreak EGC starts to increase. The sea ice contribution builds up more gradually than the shelfbreak EGC and reaches its maximum in March. Annual volume transports of the separated EGC and the NIJ are rather stable while the shelfbreak EGC shows variability on the order of ± 1 Sv, associated with wind stress curl changes south of Iceland. This is, to some extent, influenced by the large-scale atmospheric circulation. On seasonal and interannual bases an anticorrelation between the shelfbreak EGC and the separated EGC has been simulated which confirms earlier findings [*Köhl et al*., 2007; *Harden et al*., 2016]. The liquid freshwater transports are generally highly linked with volume transport changes (mainly of the shelfbreak EGC) where larger southward volume and freshwater transports go hand in hand. The model freshwater transports are substantially lower than the observations suggest due to a salt bias in this simulation. Although this salt bias offsets the

mean transports, its effect on the variability is weak since freshwater transports are highly linked to the volume transport changes.

The Lagrangian particles back-tracked from the Denmark Strait overflow ($\sigma_0 > 28.0$ kg/m^3) confirm that several branches contribute to the DSOW in agreement with current observations [*Våge et al.*, 2013; *Harden et al.*, 2016] and Eulerian results. Most of these particles follow the shelfbreak EGC, which flows along the coast of Greenland toward the Denmark Strait. The trajectories of the separated EGC suggest two sources: the first via the Blosseville Recirculation and the shelfbreak EGC, and the second via a branch on the western side of the Kolbeinsey Ridge also originating from the shelfbreak EGC. The sources for the NIJ originate mainly from the NIIC and water mass transformation north of Iceland and thus provides additional evidence and insights to the hypothesized overturning loop [*Våge et al.*, 2011] for the first time in a realistic model setup. This overturning occurs mainly along the northern Iceland shelfbreak and less in the central Iceland Sea, in contrast to recent studies [*Våge et al.*, 2011, 2015]. Due to the existence of this overturning loop, changes in the Atlantic Inflow through Denmark Strait can potentially alter the formation rates or properties of the NIJ, which provides the densest portion to the DSOW. Those changes in the DSOW have the potential to alter the AMOC [*Behrens et al.*, 2013]. Therefore, observations of the Atlantic Inflow through Denmark Strait and north of Iceland could serve as key locations to monitor long-term DSOW and thus AMOC changes. This could be could be highly relevant if meltwater fluxes from Greenland continue to increase [*Böning et al.*, 2016].

Unfortunately, our simulation ends in 2009 due to the availability of atmospheric boundary conditions and prevents a more detailed comparison with available observations. However, we present the most detailed analysis about the upstream sources of the DSOW and their variability from seasonal to interannual time scale to date.

Acknowledgments

The data, which have been used in this manuscript, can be made available upon request from the author. We would like to acknowledge comments and support of Graham Rickard, Helen Macdonald, and Dr. Alexandra Gronholz. The simulations and diagnostics for this publication have been performed using resources of the "Norddeutscher Verbund für Hoch- und Höchstleistungsrechnen" (HLRN) and NIWA HPCF facilities, which we are grateful for. The author wish to acknowledge use of the Ferret program for analysis and graphics in this paper. Ferret is a product of NOAA's Pacific Marine Environmental Laboratory. (Information are available at http://ferret.pmel.noaa.gov/Ferret/.) Support for this project was provided by the following sources: the New Zealand funded Deep South National Science Challenge; the Norwegian Research Council under grant agreement 231647 (KV); the Bergen Research Foundation (KV); and the European Union 7th—Framework Program (FP7 2007–2013) under grant agreement 308299 (NACLIM project, KV).

References

Bamber, J., M. Van Den Broeke, J. Ettema, J. Lenaerts, and E. Rignot (2012), Recent large increases in freshwater fluxes from Greenland into the North Atlantic, *Geophys. Res. Lett.*, *39*, L19501, doi:10.1029/2012GL052552.

Barnier, B., et al. (2006), Impact of partial steps and momentum advection schemes in a global ocean circulation model at eddy-permitting resolution, *Ocean Dyn.*, *56*(5–6), 543–567, doi:10.1007/s10236-006-0082-1.

Behrens, E. (2013), The oceanic response to Greenland melting: The effect of increasing model resolution, dissertation, 166 pp., Christian-Ablrechts-Univ., Kiel, Germany. [Available at http://macau.uni-kiel.de/receive/dissertation_diss_00013684.]

Behrens, E., A. Biastoch, and C. W. Böning (2013), Spurious AMOC trends in global ocean sea-ice models related to subarctic freshwater forcing, *Ocean Modell.*, *69*, 39–49, doi:10.1016/j.ocemod.2013.05.004.

Belkin, I. M. (2004), Propagation of the "Great Salinity Anomaly" of the 1990s around the northern North Atlantic, *Geophys. Res. Lett.*, *31*, L08306, doi:10.1029/2003GL019334.

Belkin, I. M., S. Levitus, J. Antonov, and S.-A. Malmberg (1998), "Great Salinity Anomalies" in the North Atlantic, *Prog. Oceanogr.*, *41*(1), 1–68, doi:10.1016/S0079-6611(98)00015-9.

Biastoch, A., R. H. Käse, and D. B. Stammer (2003), The sensitivity of the Greenland-Scotland ridge overflow to forcing changes, *J. Phys. Oceanogr.*, *33*(11), 2307–2319.

Blanke, B., M. Arhan, G. Madec, and S. Roche (1999), Warm water paths in the Equatorial Atlantic as diagnosed with a general circulation model, *J. Phys. Oceanogr.*, *29*(11), 2753–2768, doi:10.1175/1520-0485(1999)029 < 2753:WWPITE>2.0.CO;2.

Böning, C. W., E. Behrens, A. Biastoch, K. Getzlaff, and J. L. Bamber (2016), Emerging impact of Greenland meltwater on deepwater formation in the North Atlantic Ocean, *Nat. Geosci.*, *9*(7), 523–527, doi:10.1038/NGEO2740.

Bourdallé-Badie, R., and A. Treguier (2006), *A Climatology of Runoff for the Global Ocean-Ice Model ORCA025*., Mercator Rep., MOO-RP-425-366-MER, Mercator-Ocean, Toulouse, France.

Chelton, D. B., M. G. Schlax, R. M. Samelson, and R. A. de Szoeke (2007), Global observations of large oceanic eddies, *Geophys. Res. Lett.*, *34*, L15606, doi:10.1029/2007GL030812.

Dai, A., and K. E. Trenberth (2002), Estimates of freshwater discharge from continents: Latitudinal and seasonal variations, *J. Hydrometeorol.*, *3*(6), 660–687.

Debreu, L., C. Vouland, and E. Blayo (2008), AGRIF: Adaptive grid refinement in Fortran, *Comput. Geosci.*, *34*(1), 8–13, doi:10.1016/j.cageo.2007.01.009.

de Steur, L., E. Hansen, R. Gerdes, M. Karcher, E. Fahrbach, and J. Holfort (2009), Freshwater fluxes in the East Greenland Current: A decade of observations, *Geophys. Res. Lett.*, *36*, L23611, doi:10.1029/2009GL041278.

de Steur, L., R. S. Pickart, A. Macrander, K. Våge, B. Harden, S. Jónsson, S. Østerhus, and H. Valdimarsson (2016), Liquid freshwater transport estimates from the East Greenland Current based on continuous measurements north of Denmark Strait, *J. Geophys. Res. Oceans*, *122*, 93–109, doi:10.1002/2016JC012106.

Dickson, R. R., and J. Brown (1994), The production of North Atlantic Deep Water: Sources, rates, and pathways, *J. Geophys. Res.*, *99*(C6), 12,319–12,341, doi:10.1029/94JC00530.

Dickson, R. R., J. Meincke, S.-A. Malmberg, and A. J. Lee (1988), The "great salinity anomaly" in the Northern North Atlantic 1968–1982, *Prog. Oceanogr.*, *20*(2), 103–151, doi:16/0079-6611(88)90049-3.

Fichefet, T., and M. A. M. Maqueda (1997), Sensitivity of a global sea ice model to the treatment of ice thermodynamics and dynamics, *J. Geophys. Res.*, *102*(C6), 12,609–12,646, doi:10.1029/97JC00480.

Fischer, J., et al. (2015), Intra-seasonal variability of the DWBC in the western subpolar North Atlantic, *Prog. Oceanogr.*, *132*, 233–249, doi:10.1016/j.pocean.2014.04.002.
Gary, S. F., S. M. Lozier, and C. W. Böning (2011), Deciphering the pathways for the deep limb of the Meridional Overturning Circulation, *Deep Sea Res., Part II*, *58*(17–18), 1781–1797, doi:10.1016/j.dsr2.2010.10.059.
Glessmer, M. S., T. Eldevik, K. Våge, J. E. Øie Nilsen, and E. Behrens (2014), Atlantic origin of observed and modelled freshwater anomalies in the Nordic Seas, *Nat. Geosci.*, *7*(11), 801–805, doi:10.1038/ngeo2259.
Haak, H. (2003), Formation and propagation of great salinity anomalies, *Geophys. Res. Lett.*, *30*(9), 1473, doi:10.1029/2003GL017065.
Hallberg, R. (2013), Using a resolution function to regulate parameterizations of oceanic mesoscale eddy effects, *Ocean Modell.*, *72*, 92–103.
Harden, B. E., et al. (2016), Upstream sources of the Denmark Strait Overflow: Observations from a high-resolution mooring array, *Deep Sea Res., Part I*, *112*, 94–112, doi:10.1016/j.dsr.2016.02.007.
Jochumsen, K., D. Quadfasel, H. Valdimarsson, and S. Jónsson (2012), Variability of the Denmark Strait overflow: Moored time series from 1996–2011, *J. Geophys. Res.*, *117*, C12003, doi:10.1029/2012JC008244.
Jochumsen, K., M. Köllner, D. Quadfasel, S. Dye, B. Rudels, and H. Valdimarsson (2015), On the origin and propagation of Denmark Strait overflow water anomalies in the Irminger Basin, *J. Geophys. Res. Oceans*, *120*, 1841–1855, doi:10.1002/2014JC010397.
Jónsson, S. (1999), The circulation in the northern part of the Denmark Strait and its variability, *ICES Rep. C.*, 9 pp.
Jónsson, S. (2004), A new path for the Denmark Strait overflow water from the Iceland Sea to Denmark Strait, *Geophys. Res. Lett.*, *31*, L03305, doi:10.1029/2003GL019214.
Jonsson, S., and H. Valdimarsson (2012), Hydrography and circulation over the southern part of the Kolbeinsey Ridge, *ICES J. Mar. Sci.*, *69*(7), 1255–1262, doi:10.1093/icesjms/fss101.
Köhl, A. (2010), Variable source regions of Denmark Strait and Faroe Bank Channel overflow waters, *Tellus, Ser. A*, *62*(4), 551–568, doi:10.1111/j.1600-0870.2010.00454.x.
Köhl, A., R. H. Käse, D. Stammer, and N. Serra (2007), Causes of changes in the Denmark Strait Overflow, *J. Phys. Oceanogr.*, *37*(6), 1678–1696, doi:10.1175/JPO3080.1.
Koszalka, I. M., T. W. N. Haine, and M. G. Magaldi (2013), Fates and travel times of Denmark Strait Overflow Water in the Irminger Basin, *J. Phys. Oceanogr.*, *43*(12), 2611–2628, doi:10.1175/JPO-D-13-023.1.
Large, W., and S. Yeager (2009), The global climatology of an interannually air-sea flux data set, *Clim. Dyn.*, *33*, 341–364.
Logemann, K., J. Ólafsson, Á. Snorrason, H. Valdimarsson, and G. Marteinsdóttir (2013), The circulation of Icelandic waters—A modelling study, *Ocean Sci.*, *9*(5), 931–955, doi:10.5194/os-9-931-2013.
Macrander, A., R. Käse, U. Send, H. Valdimarsson, and S. Jónsson (2007), Spatial and temporal structure of the Denmark Strait Overflow revealed by acoustic observations, *Ocean Dyn.*, *57*(2), 75–89, doi:10.1007/s10236-007-0101-x.
Madec, G. (2008), NEMO the Ocean Engine, *Tech. Rep. Notes de l'IPSL*, 27(1288–1619), 193.
Mastropole, D., R. S. Pickart, H. Valdimarsson, K. Våge, K. Jochumsen, and J. Girton (2016), On the hydrography of Denmark Strait, *J. Geophys. Res. Oceans*, *122*, 306–321, doi:10.1002/2016JC012007.
Mauritzen, C. (1996), Production of dense overflow waters feeding the North Atlantic across the Greenland-Scotland Ridge. Part 1: Evidence for a revised circulation scheme, *Deep Sea Res., Part I*, *43*(6), 769–806, doi:10.1016/0967-0637(96)00037-4.
Mertens, C., M. Rhein, M. Walter, C. W. Böning, E. Behrens, D. Kieke, R. Steinfeldt, and U. Stöber (2014), Circulation and transports in the Newfoundland Basin, western subpolar North Atlantic, *J. Geophys. Res. Oceans*, *119*, 7772–7793, doi:10.1002/2014JC010019.
Orvik, K. A., and P. Niiler (2002), Major pathways of Atlantic water in the northern North Atlantic and Nordic Seas toward Arctic, *Geophys. Res. Lett.*, *29*(19), 1896, doi:10.1029/2002GL015002.
Rudels, B., E. Fahrbach, J. Meincke, G. Budéus, and P. Eriksson (2002), The East Greenland Current and its contribution to the Denmark Strait overflow, *ICES J. Mar. Sci.*, *59*(6), 1133–1154, doi:10.1006/jmsc.2002.1284.
Send, U., M. Lankhorst, and T. Kanzow (2011), Observation of decadal change in the Atlantic meridional overturning circulation using 10 years of continuous transport data, *Geophys. Res. Lett.*, *38*, L24606, doi:10.1029/2011GL049801.
Swift, J. H., and K. Aagaard (1981), Seasonal transitions and water mass formation in the Iceland and Greenland seas, *Deep Sea Res., Part A*, *28*(10), 1107–1129, doi:10.1016/0198-0149(81)90050-9.
Swift, J. H., K. Aagaard, and S.-A. Malmberg (1980), The contribution of the Denmark strait overflow to the deep North Atlantic, *Deep Sea Res., Part A*, *27*(1), 29–42, doi:10.1016/0198-0149(80)90070-9.
Våge, K., R. S. Pickart, M. A. Spall, H. Valdimarsson, S. Jónsson, D. J. Torres, S. Østerhus, and T. Eldevik (2011), Significant role of the North Icelandic Jet in the formation of Denmark Strait overflow water, *Nat. Geosci.*, *4*(10), 723–727, doi:10.1038/ngeo1234.
Våge, K., R. S. Pickart, M. A. Spall, G. W. K. Moore, H. Valdimarsson, D. J. Torres, S. Y. Erofeeva, and J. E. Ø. Nilsen (2013), Revised circulation scheme North of the Denmark Strait, *Deep Sea Res., Part I*, *79*, 20–39, doi:10.1016/j.dsr.2013.05.007.
Våge, K., G. W. K. Moore, S. Jónsson, and H. Valdimarsson (2015), Water mass transformation in the Iceland Sea, *Deep Sea Res., Part I*, *101*, 98–109, doi:10.1016/j.dsr.2015.04.001.
Vinje, T. (2001), Fram Strait ice fluxes and atmospheric circulation: 1950–2000, *J. Clim.*, *14*(16), 3508–3517, doi:10.1175/1520-0442(2001)014<3508:FSIFAA>2.0.CO;2.
von Appen, W.-J., I. M. Koszalka, R. S. Pickart, T. W. N. Haine, D. Mastropole, M. G. Magaldi, H. Valdimarsson, J. Girton, K. Jochumsen, and G. Krahmann (2014), The East Greenland Spill Jet as an important component of the Atlantic Meridional Overturning Circulation, *Deep Sea Res., Part I*, *92*, 75–84, doi:10.1016/j.dsr.2014.06.002.
Yang, J., and L. J. Pratt (2014), Some dynamical constraints on upstream pathways of the Denmark Strait Overflow, *J. Phys. Oceanogr.*, *44*(12), 3033–3053, doi:10.1175/JPO-D-13-0227.1.